Int J Adv Manuf Technol (2017) 88:255–267
DOI 10.1007/s00170-016-8727-9

ORIGINAL ARTICLE

Deformation analysis in single-point incremental forming through finite element simulation

Yanle Li[1,2] · **William J. T. Daniel**[3] · **Paul A. Meehan**[3]

Received: 22 January 2016 / Accepted: 4 April 2016 / Published online: 23 April 2016

Abstract Incremental sheet forming (ISF) is a promising manufacturing technology in which complex 3D shapes can be formed with one simple tool. Compared to conventional forming processes, for complex shapes, it is more flexible and economical with higher formability and shorter lead time. Therefore, ISF is ideally suitable to rapid prototype and small-batch production, especially in the aerospace and biomedical sectors. Over the last decade, although the process has been experimentally studied extensively, the associated deformation mechanics is still unclear and intensive investigation is needed. The purpose of this study is to provide further knowledge of the deformation mechanics of the sheet and clarify the deformation mechanism in a typical cone-forming process through finite element (FE) simulation approach. In particular, comprehensive FE models with fine solid elements are utilised, which allow the investigation of deformation modes including stretching, bending and shearing. The FE model is firstly validated with experimental results in terms of forming forces, and then, the evolution history of all the strain components along with the effective strain is presented. The contribution of each strain component to the effective plastic strain during the cone-forming process is discussed. Moreover, the characteristic of each strain component is investigated in detail. It is confirmed from the FE simulation that the deformation modes in the ISF process are a combination of shearing, bending and stretching, although the quantitative contributions in each direction are varied. The effect of step-down size on material plastic deformation as well as formability is also investigated.

Keywords Incremental sheet forming · Forming force · Formability · Prediction · Shear · Bending

✉ Yanle Li
yanle.li@sdu.edu.cn

[1] School of Mechanical Engineering, Shandong University, Jinan 250061, China

[2] Key Laboratory of High Efficiency and Clean Mechanical Manufacture, Ministry of Education, Shandong University, Jinan 250061, China

[3] School of Mechanical and Mining Engineering, The University of Queensland, St Lucia, Brisbane QLD 4072, Australia

1 Introduction

Incremental sheet forming (ISF) is a flexible, economical low-volume production process which has received much attention in aerospace [1] and biomedical [2] manufacturing sectors over the last two decades. By using this process, complex parts can be formed directly from CAD data with a minimum of specialised tooling. Therefore, it has a high potential for rapid prototyping applications and small-quantity production. Although substantial research has been performed by researchers in the past few years, there still remains a lack of intensive understanding of the deformation mechanics of the forming process which are critical in optimising the process for better output qualities.

The deformation mechanics behind ISF have been investigated both analytically and experimentally [3–6]. It has been widely accepted that ISF is characterised by higher formability compared with other conventional forming processes [7, 8]. Silva et al. [3–5] extensively analysed the single-point incremental forming by means of a membrane approach. A closed-form analytical model was firstly presented, which provides insight to explain the fundamentals behind the fracture of material and the enhanced overall formability of ISF. Lu et al. [9, 10] further discussed the role of friction and

through-thickness shear analytically from the stress state point of view. It was claimed that the effect of through-thickness shear caused by friction is two sided. The higher shear stress not only potentially enhances the deformation stability but also increases the stress triaxiality and reduces the formability at the same time. Although the developed analytical model shows a qualitative agreement when compared to its predictive finite element method (FEM) and experimental results, the model uses some simplifications, such as neglecting bending effects, assuming axial symmetry and rigid perfectly plastic and isotropic materials. This limits its further applications. Emmens and Boogaard [11] summarised that bending under tensile load plays a critical role in the localised deformation of ISF process. Unlike the above approach, Mirnia and Darinia [12] analysed the deformation behaviour of a cone-forming process based on the upper bound theory. Despite that shear deformation was assumed as the main deformation mechanism, this approach was shown to be effective for predicting the tangential forming force. Based on Mirnia's work, Li et al. [13, 14] further developed the model to take into account bending and stretching deformation modes and verified the model with experimental tests. However, the contribution between each deformation modes needs to be further investigated and quantified.

The deformation mechanics have been investigated experimentally. Jackson and Allwood [6] experimentally measured the strain distributions through the thickness of the sheets along the cross-sectional plane. It was claimed that the deformation mechanism for ISF is stretching and shear in the plane perpendicular to the tool direction together with shear in the plane parallel to the tool direction. Interestingly, shear strain in the tool moving direction was measured as the greatest strain component. Eyckens et al. [15] measured the strain distribution during the deformation process by a stereovision system. It was suggested that the dominant deformation mechanism depends on the selected forming parameters (e.g., wall angle and step-down size). The author also studied the strain behaviour through a FE model. It was found that a good qualitative agreement has been obtained for the surface strain, but the through-thickness shear was not fully captured. However, it is still difficult to reveal the detailed deformation history behind the ISF solely through experimental works due to its highly localised characteristic. Therefore, computer models especially FE technology are widely applied to investigate this process. Despite the advances in the finite element analysis for modelling of metal-forming processes and the improvements in computational speed, the numerical simulation of the single-point incremental forming (SPIF) process remains a challenging task. The continuous changing localised plastic deformation and the complex tool path result in a significant computation time. Lasunon and Knight [16] confirmed that the FE model can be used to investigate various capabilities of ISF processes by validation with experimental testing with truncated pyramids. Yamashita et al. [17] investigated the applicability of the dynamic explicit finite element code DYNA3D for the simulation of an incremental sheet-forming process of quadrangular pyramids. The effect of tool path on deformation behaviour was discovered, which shows that the starting forming position should be at one of the corners of the final product. Ma and Mo [18] found that the FE model based on solid elements is more suitable to simulate the SPIF in terms of deformation prediction. Dejardin et al. [19] conducted a numerical analysis using LS-DYNA software to predict the springback effect through the cut ring method. It was found that the finite element model with shell elements is not suitable for all tool path strategies to capture the transverse shear behaviour of the sheet. Future work with a FE model using elements able to properly account for the shear component is suggested. Recently, Smith et al. [20] analysed the deformation mechanics of both single-point and accumulative double-sided incremental forming (ADSIF) process by FE simulation using LS-DYNA explicit software. Solid elements were used in the described FE model and evolution history to show plastic strain, hydrostatic pressure and shear strains parallel and perpendicular to tool motion. The authors concluded that the ADSIF could present greater plastic strains, through-thickness shear strains and greater hydrostatic pressure than in SPIF and suggested that this might be the reasons for the increased formability in ADSIF. Al-Ghamdi and Hussain [20] investigated the effect of relative value of tool radius and blank thickness (i.e., R/T_B) on the formability for SPIF through both experimental and FE simulation. A threshold radius $R_c \approx 2.2T_B$ was identified to achieve the conducive deformation condition with high compression with low-damage constitutes.

Previous FE investigations mostly use shell element considering the reduced computation time, but it is not reasonable to represent the actual deformation mechanism during the forming process. To this end, the purpose of the present work is to develop a comprehensive FE model with fine solid elements and investigate the detailed deformation mechanism during the ISF process. In particular, the evolution history and amplitudes of all the strain components are discussed. Also, deformation modes of shear, bending and stretching are examined. Section 2 briefly presents the modelling and experimental setup for the forming of a truncated cone shape. The validation of the FE model with measured forces is provided in Sect. 3. Then, the results and the associated discussion are presented in Sect. 4, followed by the conclusions in Sect. 5.

2 FE modelling

As the ISF process involves continuously changing localised plastic deformation as well as large material plastic

deformation, the simulation must consider high non-linearity and large plastic deformation. LS-DYNA is a general-purpose finite element program capable of simulating complex non-linear problems and can accurately solve dynamic problems which have 3D elastic–plastic large deformation using explicit time integration. Therefore, in the present work, the finite element code of LS-DYNA was used to perform the numerical simulation.

In the presented FE model, forming tools were modelled as rigid bodies and the tool path was predefined using CAM software. As a benchmark study, the forming process of the truncated cone was simulated. During the process, the shape was formed layer by layer with a series of successive contours. The vertical distance to the adjacent contour was defined as step-down size Δz. Due to changing contact positions and the three-dimensional tool path, simulations with only a quarter or a half of the whole part are not recommended [6]. Therefore, a fully three-dimensional model needs to be realised. To accurately predict the through-thickness shear and bending effect of the deformed sheet, the element type of SOLID164 is used in the current model and five elements are meshed through the thickness direction. The SOLID164 element is an eight-node brick element, and the default one-point integration option was chosen due to savings on computer time and robustness in cases of large deformations. The initial meshing configuration of the metal sheet is shown in Fig. 1 with an enlarged view of the selected small region *d* plotted at the top right corner. Specifically, the sheet was divided into three regions which allow having different meshing of each region. For the region which will be contacting with the tool (region *B*), the elements are arranged with the same size at 1 mm radially and meshed into 400 elements circumferentially, which correspond to the size between 0.7 and 1.2 mm. Region *A* at the inner base of the cone was meshed freely as the transition zone towards the centre point of the sheet. For the rest of the sheet

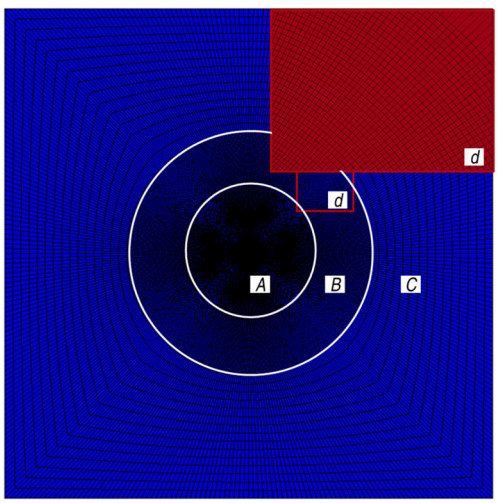

Fig. 1 The initial meshing configuration of the metal sheet with enlarged view at the *right top corner*

out of the contact region, it was meshed with relatively large element size as the deformation in this area is quite small and has little effect for the final results. By using this strategy, the localised deformation in the contact region in both radial and circumferential directions can be captured without much distortion of the elements. As a result, the current meshing is able to increase the localised precision of prediction as well as reduce the computing expenditure. The general geometry of the sheet is square with dimension 300 × 300 mm, and thus, it is meshed with 175,000 solid elements. In terms of the boundary conditions in the forming process, nodes that belong to the four edges of the squared sheet are constrained in all degrees of freedom. The diameter of the forming tool was 30 mm in the presented models.

The metal used in the simulation was the aluminium alloy 7075-O sheet with a thickness of 1.6 mm. It was confirmed from tensile tests that the material can be considered isotropic since deviations of the stress–strain behaviour in different directions (rolling, diagonal and transverse) are small. Therefore, the material could be modelled using Swift's isotropic strain hardening law of $\sigma = K(\varepsilon_0 + \varepsilon)^n$. The detailed mechanical parameters are listed in Table 1, which were determined from previous material tests [21]. Only the data of the stress–strain curve form tensile test before fracture was imported into the LS-DYNA software, and the strains beyond the localised point were automatically determined by the LS-DYNA code. In the code, the von Mises (isotropy) yield function was used to determine the plastic flow when the stress is on the yield surface. Based on previous findings, the highest accuracy in FE modelling will be achieved, whilst mixed isotropic-kinematic hardening model of Voce–Ziegler has been selected. But, since this is not the main contribution of this thesis and the limit of the material testing facility, a simple material model was used in this FE model. In order to improve the simulation efficiency, the virtual forming speed was scaled up by 100 times, in which the ratio of the kinetic energy to the total internal energy can be controlled within 1 % to ensure a quasi-static forming process. The determination of friction is based on our previous work [22] during a groove-forming process. Specifically, the evaluation of friction coefficients

Table 1 Mechanical properties of aluminium 7075-O sheets with 1.6-mm thickness

Material	7075-O
Density (t/mm^3)	2.81×10^{-9}
Young's modulus (GPa)	70
Poisson's ratio	0.33
Tensile yield strength (MPa)	92
Ultimate tensile strength (MPa)	198
Plastic coefficient *K*	352.58
Hardening exponent *n*	0.221

was conducted by calculating the absolute value of the ratios between horizontal and vertical components in the central area of the specimens, which has been widely used by Durante [23] and Hamilton [24]. According to experimental results, the absolute value of the ratios shows a slightly growing tendency in the middle area of the groove caused by the continual increase of the groove depth, which requires more forces to stretch the sheet during each travel. An average value of 0.18 has been calculated as the average friction coefficient; hence, this value was used in the FE model. In order to improve the simulation efficiency, the virtual forming speed is scaled up by 100 times, in which the ratio of kinematic energy to total energy can be controlled within a limited value.

3 Validation of the FE model

The proposed FE model with solid elements is validated by comparing the predicted forming forces with experimental results. In the present work, the forming tests were performed on a state-of-the-art machine dedicated for the ISF process designed by AMINO Corporation as shown in Fig. 2. The machine allows mould-based forming for a maximum size of 2100 × 1450 × 550 mm with a FANUC controller for precise control. The movement of the two horizontal axes (*X* and *Y*) can have a maximum speed of 60 m/min with a repeatability of ±0.05 mm. The vertical (*Z*) axis is driven by an AC servo motor with the power of 1 kW that allows a maximum acting force of 3 kN. Hemispherical tools with the diameters ranging from 10 to 30 mm were used to deform the material. The tip of each tool is tungsten carbide, and the body is made of K110 steel which was hardened and tempered to HRC60. The forming tool was set not to rotate in this study for all the tests.

As shown in Fig. 2b, a force sensor was mounted between the spindle and the tool holder to alleviate the indirect impact from other structures. The force sensor model K6D175-50 was manufactured by ME-Meßsysteme GmbH, which allows measuring the three orthogonal force and three torque components at the same time. The six-channel signals were recorded with two NI 9237 data loggers and post-processed with the LabVIEW SignalExpress software. The forces measured with this system shown in Fig. 3 were for a 1.6-mm thick aluminium sheet. In this test, as shown in Fig. 2a, a truncated cone with an outer diameter of 140 mm was formed with a wall angle of 60° and step-down size of 0.5 mm at a constant speed of 4000 mm/min. The sheet material used in the present study was aluminium alloy 7075-O sheet with different thickness and was cut into 300 × 300-mm-sized samples.

In Fig. 3, the predicted forming force by the proposed FEM model was compared with the force measured by the force sensor. It can be seen that the predicted forces both in vertical and horizontal components were in good agreement with measured values, except that the vertical force is slightly overestimated at the initial stage of the process. It should be noted that due to the similarity of the two horizontal components (F_x and F_y), only F_x was plotted for comparison. The maximum value of F_x can be considered as the tangential forming force, as it represents the force at 90°, where $F_y = 0$. The same trend can be observed from both experimental and FE simulation results. In one contour, horizontal force F_x changes in a sinusoidal way between their maximum and minimum values due to the current tool position relative to the global absolute axis of the truncated cone. In contrast with the horizontal force, the amplitude of the vertical force increases during the early phase of the process with small fluctuations between each contour and tends to become steady with the further increase of the formed depth. The small deviation of the modelled and measured force results for the peak values may be due to three reasons: (1) 7075-O aluminium alloy is strain rate sensitive, and artificially increasing the working speed might adversely affect the accuracy of predicted forming forces; (2) although the same tool path trajectory is defined in the FE model, the time increment between two adjacent points is set constant, which may result in a slight variation of the forming speed. This is reflected from the offset of the forces obtained from experimental and FE simulation values shown in Fig. 3. (3) Model boundary conditions might not have corresponded to reality. In the simulation, the edges are completely fixed, whilst it may be deflected during actual

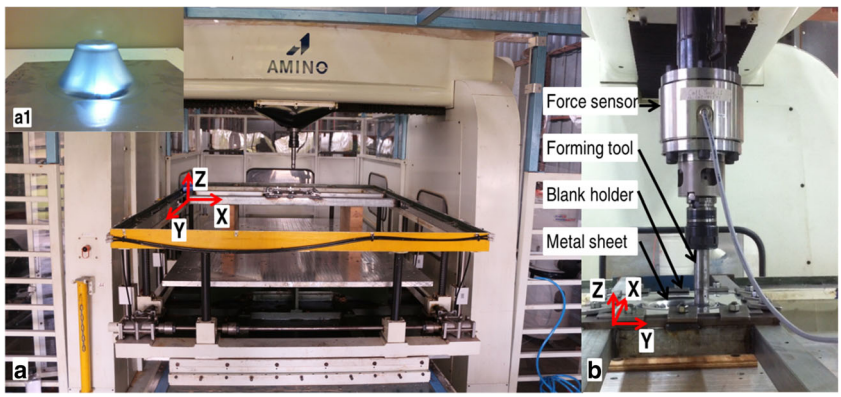

Fig. 2 ISF configuration, **a** amino incremental forming machine, **a1** a formed truncated cone and **b** the implemented force sensor

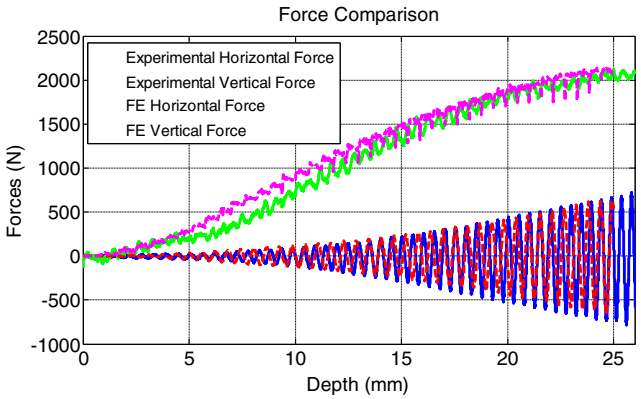

Fig. 3 Force comparison between FE model and experimental results (angle = 60, step-down = 0.5mm)

forming processes. However, for the investigation of strain behaviour and deformation mechanism in this process, the predicted forming forces during the cone-forming process are acceptable as conservative measures, although these aspects could be further investigated for developing an accurate force prediction model.

4 Results

In order to investigate and quantify the local deformation behaviour in the cone-forming process, four distinct sections (1 to 4 from outer to inner as shown in Fig. 4) along the inclined wall were selected. Furthermore, strain values with the variation along thickness direction at each of these sections were also investigated by checking upper element (the side in contact with the forming tool), lower element (the side without contact with the forming tool) and the middle element. It should be noted that the following strain values are presented in the local Cartesian coordinate system as marked in Fig. 4. The direction perpendicular to the tool motion and along the inclined wall is defined as 1, whilst forming direction (circumferential direction) is defined as 2 and thickness direction as 3.

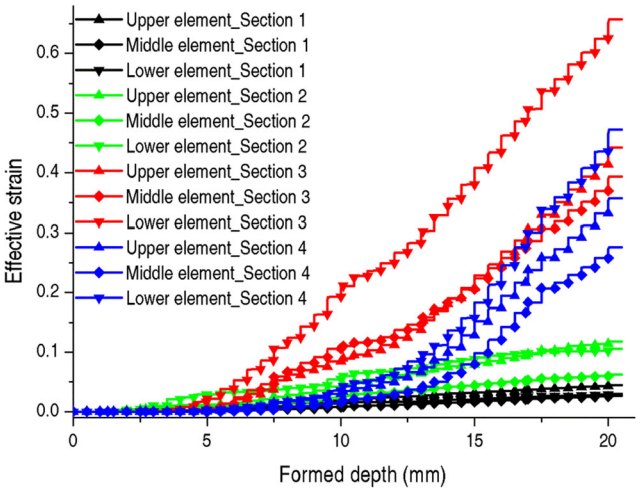

Fig. 5 Plastic strain evolution in cone-forming process for upper and lower elements from sections 1 to 4 (as marked in Fig. 4)

The cross-sectional view of the FE model is presented in the global Cartesian coordinate system as marked at the lower left corner in the following figures. In this section, the evolution history of each strain component and their contributions to the effective plastic strain during the cone-forming process with the step-down size of 0.5 mm will be provided. Since different values of step-down could be used in industrial applications, the effect of step-down size on material plastic deformation as well as formability is also investigated.

4.1 Evolution history of effective strain

Figure 5 shows the evolution of effective strain in the cone-forming process simulation for sections 1 to 4, from the outer side (section 1) to the inner side (section 4) of the cone. At each section, the history of effective plastic strain of both upper element and lower element are plotted as a function of the forming depth. The figure shows that the effective strain values for all the elements are increasing continuously with the forming depth for all sections, which reflects the inherent

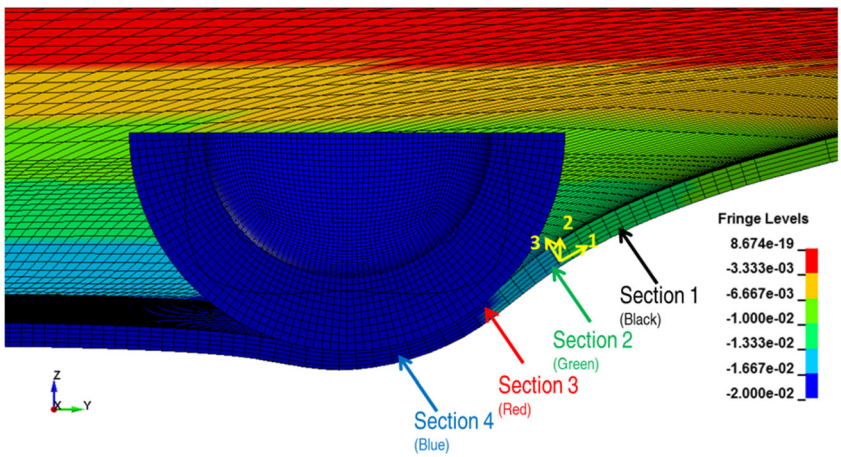

Fig. 4 Four selected critical sections along the cross section to check the strain values

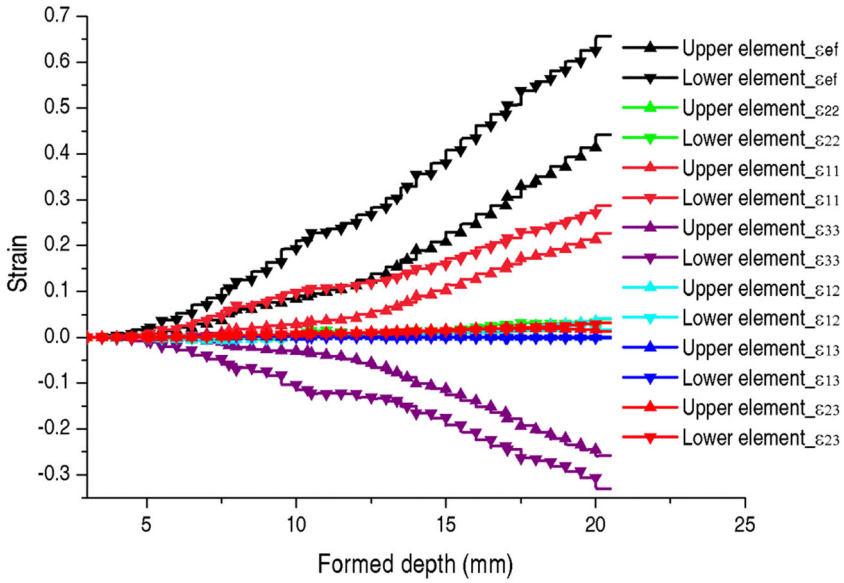

Fig. 6 Evolution history of all strain components at section 3

mechanics of incremental forming process. However, the effective plastic strain at sections 1 and 2 are relatively small (less than 0.1) compared with other sections. This may be explained by the fact that these two sections are located close to the outer edge of the cone where no substantial plastic deformation is expected. These already deformed regions would not be further affected by the forming process. It confirms the inherent characteristic of the ISF process that the major deformation of the sheet is localised around the forming tool. For this reason, it can also be noticed that the other two sections (3 and 4) present more severe plastic deformation, which correspond to the current local contact zone in the current tool path. Additionally, by checking the effective strain value for both sides, an obvious difference can be noticed between upper and lower elements especially for sections 3 and 4. This difference indicates the existence of the bending effect. Previous research, from both simulation [19] and experimental [6] studies, have proved that material bending under stretching was the primary reason for larger plastic strain on the outer side of the sheet. According to the bending theory [25], with the same thickness, the element with a smaller local radius results in a larger bending strain. In the case of the cone-forming process, the elements at the base corner must have the smallest radius which is represented as Sect. 3 in the presented model. This analysis is consistent with the FE simulation as shown in Fig. 5 that the largest difference of effective strain between upper and lower values occurred at Sect. 3.

4.2 Strain components

Figure 6 compares the evolution history of six strain components along with the plastic effective strain ε_{ef}. It is shown that all the values developed monotonically; therefore, it is reasonable to analyse the strain composition at a certain point. A column comparison of all six strain components and the plastic effective strain for upper, middle and lower elements at section 3 is presented in Fig. 7. These values are obtained when the forming tool is contacting with section 4 at the depth

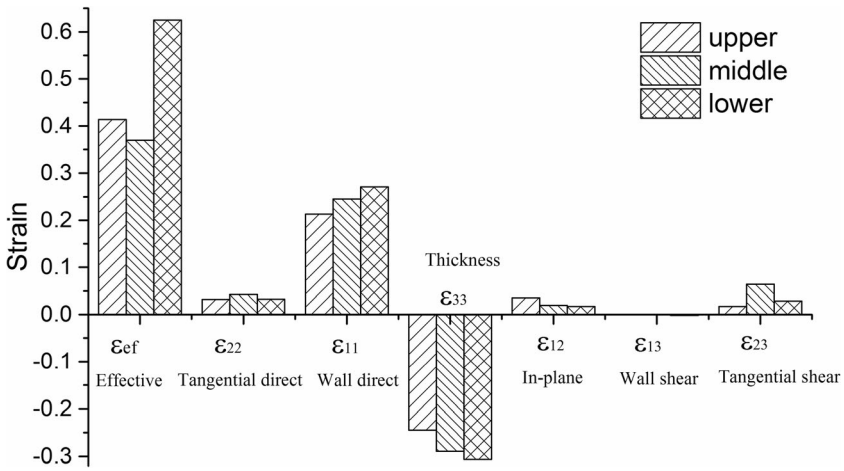

Fig. 7 Strain components for upper, middle and lower elements at section 3 at the forming depth of 20 mm

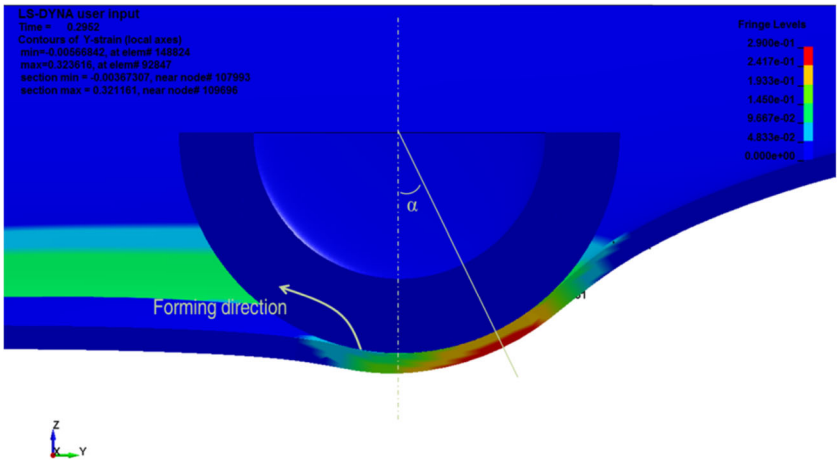

Fig. 8 Direct strain perpendicular to the forming direction (ε_{11}), on a cross section in *ZY* plane directly below the tool

of 20 mm. In this study, a feature depth of 20 mm was selected due to the following reasons: (a) the long computing time for a deeper cone (110 h for the current depth), (b) the selected depth is reasonable to represent the stable deformation process considering that the failure depth is only 37 mm in the real experiment and (c) the deformation of the material is localised so the following forming process has limited effect on the deformed part. It is noted that the strain component perpendicular to the forming direction (ε_{11}) dominates the total plastic strain at the picked elements with the highest positive strain. According to the law of volume constancy, the sheet has to be thinned during this process, which is clearly confirmed by the negative thickness strain (ε_{33}) in Fig. 6. The thinning in the thickness direction could be considered as a direct indicator for the formability in ISF process since it is suggested that the fracture of sheet comes from the suppression of necking before fracture [26]. Not surprisingly, the strain values in the circumferential direction (ε_{22}) are small compared with the other two orthogonal directions as the deformation in the forming direction is symmetrical and constrained for extension.

In contrast, shear strain ε_{23} prevails greatly amongst the three shear components with negligible ε_{13}. The above results from FE simulation agree with the experimental measurement by Jackson and Allwood [6]. It is also noticed that the strain values are varying through the thickness as shown in Fig. 7. The lower element on the non-contacting surface was deformed with the highest effective strain value, which is mainly resultant from large-strain ε_{11} and thickness strain ε_{33}. However, the in-plane shear strain ε_{12} takes a significant role as part of the effective strain value at the upper element. The above detailed analysis indicates that the deformation mechanism is different in circumferential and its perpendicular directions. More specifically, the deformation mode in the circumferential (forming) direction is a combination of the transverse shear strain ε_{23} and also a comparable amount of direct

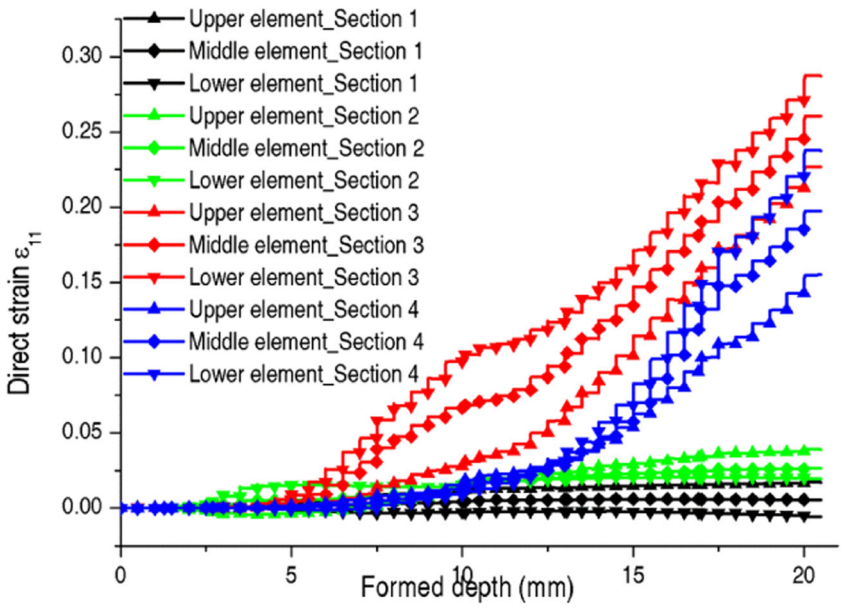

Fig. 9 Evolution of the direct strain perpendicular to tool motion (ε_{11}) of the elements from sections 1 to 4

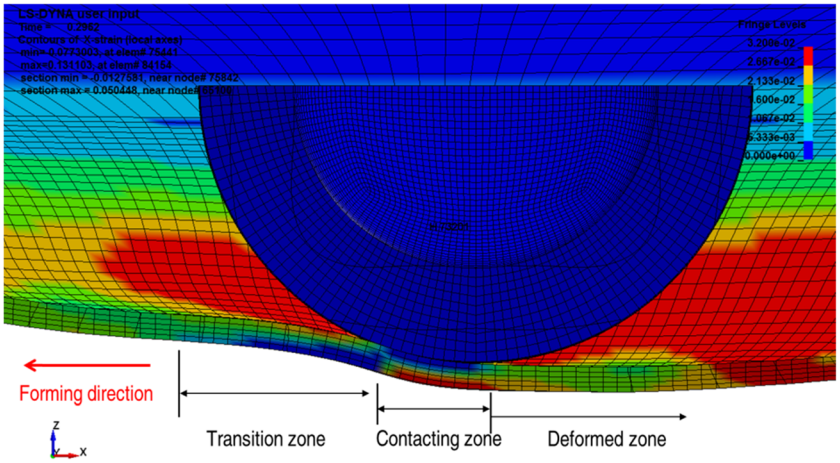

Fig. 10 Direct strain parallel to the forming direction (ε_{22}), on a cross section in *ZX* plane directly below the tool

strain ε_{22}. However, the direct strain ε_{11} governs the deformation behaviour in the direction perpendicular to the tool motion. This confirms that the formation of the inclined wall is represented by a combination of stretching and bending with substantial transverse shear. The following sections will discuss each strain components individually.

4.3 Direct strain perpendicular to the forming direction

It was confirmed from earlier discussion that the direct strain perpendicular to the forming direction and along the inclined wall ε_{11} dominates the magnitude of the plastic strain; therefore, a detailed investigation of ε_{11} is of great importance. Figure 8 shows the distribution of the direct strain ε_{11} on a cross section radially during a cone-forming process. It can be clearly seen that a circular deformation band is obtained around the bottom of the cone, which indicates that a considerable amount of direct strain is formed. By contrast, there is nearly no plastic strain of ε_{11} at the initial few contours. This is further demonstrated by Fig. 9. In this figure, the amount of ε_{11} for elements at sections 1 and 2 are smaller than 0.04, which are insignificant compared with the value of around 0.25 at section 4. In the deformation band, the maximum strain values occurred at the lower surface of the sheet and with an angle α to the axial direction of the forming tool. This is consistent with the basic bending theory that the bending strain is proportional to the distance to the middle surface. For this reason, obvious bending is recorded around this region, whilst the rest of the sheet undergoes uniform direct strain through the thickness. It is also shown that the bending strain (deviation of strain values between upper and lower elements) peaks at the forming depth of 10 mm for section 3 when the direct contact level is just above section 3. Similarly, at section 4, the bending strain is building up as the forming tool is currently contacting with this section. Therefore, it is concluded that the bending effect in the direction perpendicular to the tool motion is greatly affected by the contacting of the forming tool. More specifically, the bending strain increases with the approaching of the tool and achieves the maximum value when the region is currently being formed. Then, the bending strain reduces to a steady value after the passing of the forming tool.

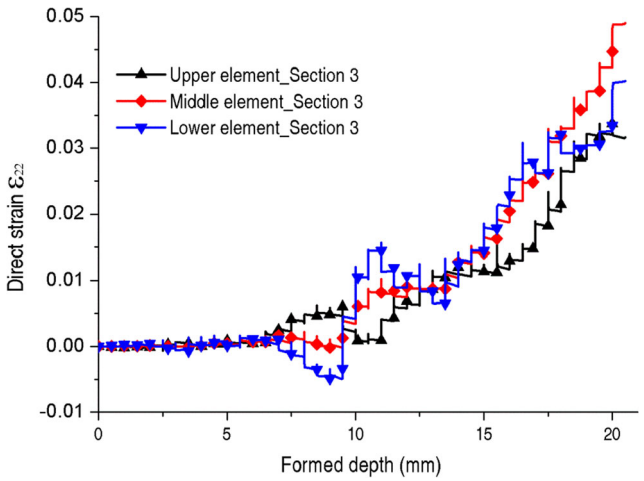

Fig. 11 Evolution of the direct strain (ε_{22}) of the elements at section 4

4.4 Direct strain parallel to the forming direction

Figure 10 shows the distribution of the strain in forming direction (ε_{22} tangential direction) along a cross-section plane. As indicated by the arrow in the figure, the tool is deforming the sheet leftwards and currently is just above the blue region on the upper surface. Based on the distribution of ε_{22}, the deformation zone around the forming tool can be divided into the following three zones: transition zone, contacting zone and deformed zone. For the elements on the upper surface, they undergo a stretching-compressing-stretching process corresponding to the three zones. In the contrast, the elements on the lower surface experience a compressing-stretching-recovering process. As a result, the bending effect is introduced due to the deviation of the strain values between upper

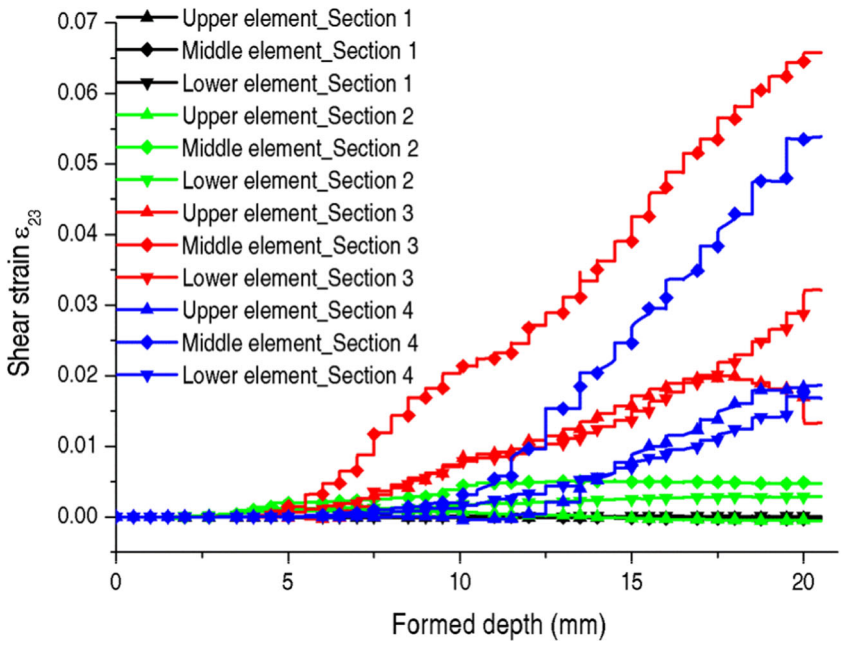

Fig. 12 Shear strain evolution parallel to the forming direction during cone-forming process for upper, middle and lower elements from sections 1 to 4

and lower elements. Figure 11 plots the evolution history of the direct strain ε_{22} of the upper, middle and lower elements at section 4. The plot further confirms that the bending effect does exist when the sheet is plastically deformed. However, it is noticed that the bending direction is alternating as the tool passes through the elements.

4.5 Shear strain parallel to forming direction

Figure 12 presents the magnitude of the shear strain component in forming direction for upper, middle and lower elements for all four selected sections. Similar with the effective plastic strain, the magnitudes of shear strain at sections 1 are small because of the small amount of plastic deformation. However, as deformation accrues, much larger values of the shear strain can be obtained at sections 3 and 4. The above observation suggests that the shear strain in the forming direction is proportional to the increase of the plastic strain through the forming process. Additionally, at all of these sections, the magnitudes of the shear strain in the forming direction at upper elements are comparable to that at lower elements, whereas the middle elements experience much larger shear deformation. In particular, at the forming depth of 20 mm for section 3, the middle element takes on a value of 0.065, which is more than twice that observed in the lower element (0.030). This is clearly illustrated in Fig. 13 where a great deal of transverse shear is elicited in the middle band of the metal sheet after the forming tool passes. This is not surprising if considering the deformation along the circumferential direction as a cantilever beam. It is assumed that the sheet made up of five layers is subjected to a transverse vertical loading, so that longitudinal shear stresses must develop to prevent the

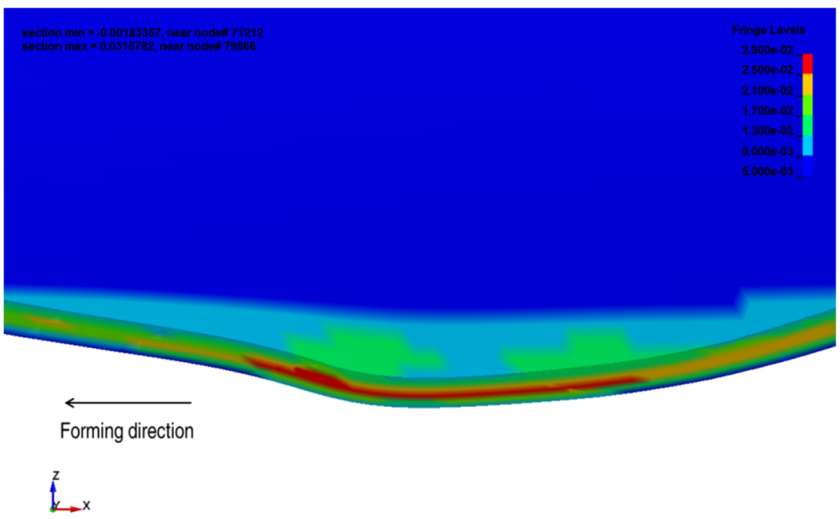

Fig. 13 Distribution of shear strain parallel to the forming direction on a cross section in *ZX* plane directly below the tool

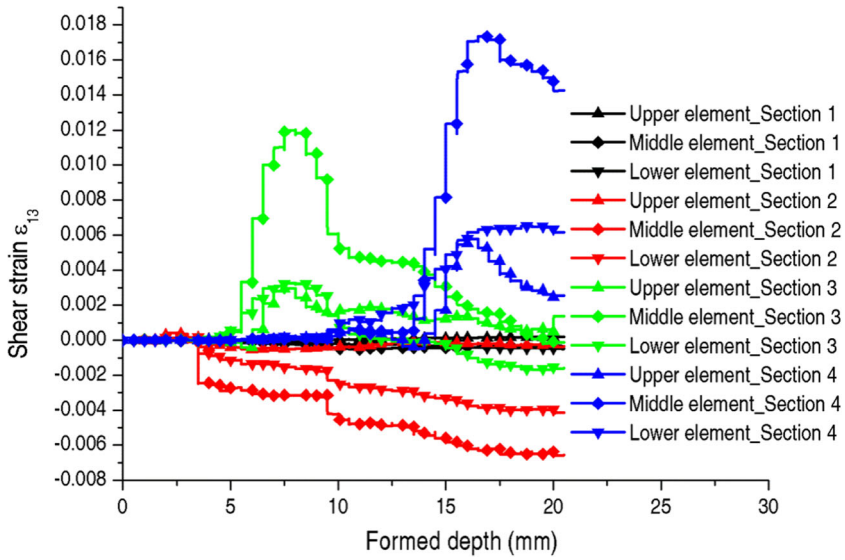

Fig. 14 Shear strain evolution perpendicular to the forming direction during cone-forming process for upper, middle and lower elements from sections 1 to 4

relative sliding between layers. In this case, there is maximum shear strain at the middle layer, whilst deformation should be much less at the top and bottom of the sheet because of the loose restraint of the material.

4.6 Shear strain perpendicular to forming direction

It should be noted the shear component perpendicular to the forming direction ε_{13} is much smaller than that of shear strain ε_{23}. Nevertheless, it is still beneficial to recognise and understand the evolution pattern of it. Unlike other strain components, as shown in Fig. 14, the evolution history of ε_{13} is not accumulating at sections 3 and 4. A peak value is obtained only when the forming tool passes through these sections and then reduces rapidly to zero and negative values. This trend is easily seen from the inspection of the change of the curvature at these sections. At the forming depth of 20 mm, as shown in Fig. 15a, the maximum positive ε_{13} occurs at section 4, which is currently being deformed where the sheet is bending upwards. Conversely, the maximum negative strain value which is represented by the blue colour takes place at section 2, where the sheet is bending downwards. Due to the symmetric geometry of the truncated cone, a circular band is made up at the same depth with section 2, which can be seen in Fig. 15b.

4.7 Shear strain in the sheet plan

As mentioned in previous section of the present work, the ISF process also produces a considerable amount of in-plane shear strain (ε_{12}). However, this strain component is not well investigated so far. Figure 16 shows that the tool tends to drag the sheet in the direction of forming, shearing it in-plane, especially at the outside radius of the contact zone when forming a cone. In fact, the flat base of the cone being formed has experienced a rigid body rotation about the vertical axis, due to this shearing. This strain is related to the foreshortening of the sheet in the forming direction as it is bent down by the approaching tool. In practice, there is also a significant variation of in-plane shear strain through the thickness due to plate twisting. The evolution history of in-plane shear strain during the cone-forming process for upper, middle and lower elements from sections 1 to 4 is shown in Fig. 17.

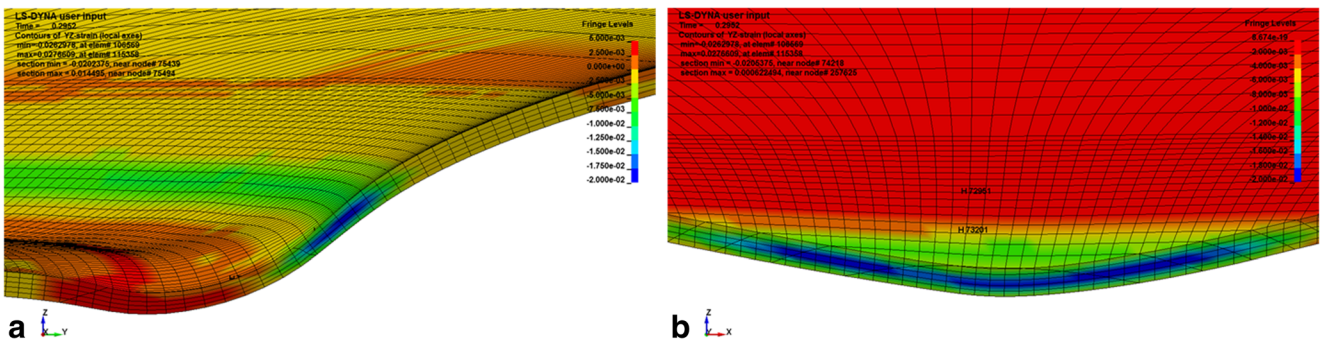

Fig. 15 Distribution of shear strain perpendicular to the forming direction on a cross section in **a** *ZY* plane and **b** *ZX* plane

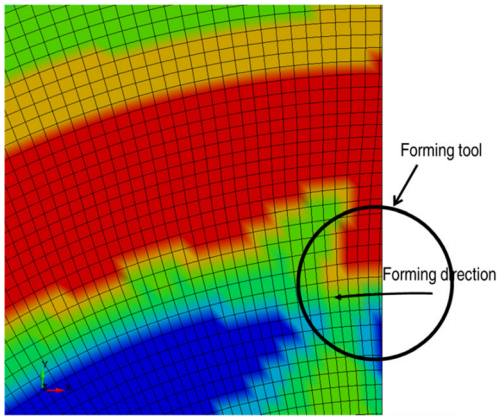

Fig. 16 Distribution of in-plane shear strain from *top view*

4.8 Effect of step-down

The effect of step-down size on the deformation mechanism during the ISF process is also investigated. Four FE simulation cases have been performed with different step-down values from 0.5 to 4.0 mm as listed in Table 2. All the simulation cases successfully reached the designed depth (40 mm) except test 1, in which large hourglass energy was generated due to the severe distortion of the elements. All calculations were carried out by a desktop PC with eight threads running simultaneously.

Figure 18 demonstrates the evolution histories of all strain components for both upper and lower elements at section 3 with the varying of step-down size from 1.0 to 4.0 mm. It can be seen that the values of all strain components are continuously increasing with the proceeding of the forming process before contacting with the forming tool and then followed by a steady stage after the forming tool has passed section 3 completely at the forming depth of 25 mm. This suggests that the deformation of the material tends to transfer from a distributed deformation to a highly localised deformation under the contact region around the forming tool. At the initial stage, different strain increments are obtained between the neighbouring contours if tool paths with different step-down sizes are adopted. Specifically, as can be seen in Fig. 18, larger-strain increments at each step are produced with larger step-down values that are enforced by the forming tool to achieve the same amount of plastic deformation through fewer increments. During the forming process, the relations between strain values of upper and lower elements are inversed for both strain ε_{11} and thickness strain ε_{33}. This is due to the changing of the bending direction in the radial direction of the sheet as the forming tool passes the section.

Figure 19 compares the strain values for the middle element at section 3 with four different step-down sizes at the forming depth of 20 mm. It is seen that that the effective plastic strain value decreases with the increase of the step-down up to 2 mm but remains the same level at 4 mm. Similar trends can be observed for the amplitude for all the direct strain components ε_{11}, ε_{22} and ε_{33} as well as the shear strain ε_{23}. However, the shear strain components ε_{12} and ε_{13} obtained their peak value at the step-down size of 2 mm, although amplitudes are small compared with other strain components. This can be due to the fact that smaller step depth size leads to smaller tool contour distance between two neighbouring contours. In the ISF process, material in the contact zone of the metal sheet is deformed by the tool end and is hardened repeatedly after each forming contour. In particular, with small Δz, the amount of already hardened material which is deformed by the forming tool in each pass is higher and may result in more redundant material flow. This leads to a great increase in the contact stress required to reach the target deformation. Consequently, higher total strain values are accumulated in the material with small step-down. Hence, with small step-down size, although the forming forces are small due to the limited strain increment in each step, the final accumulated strain may be large. As a result, the

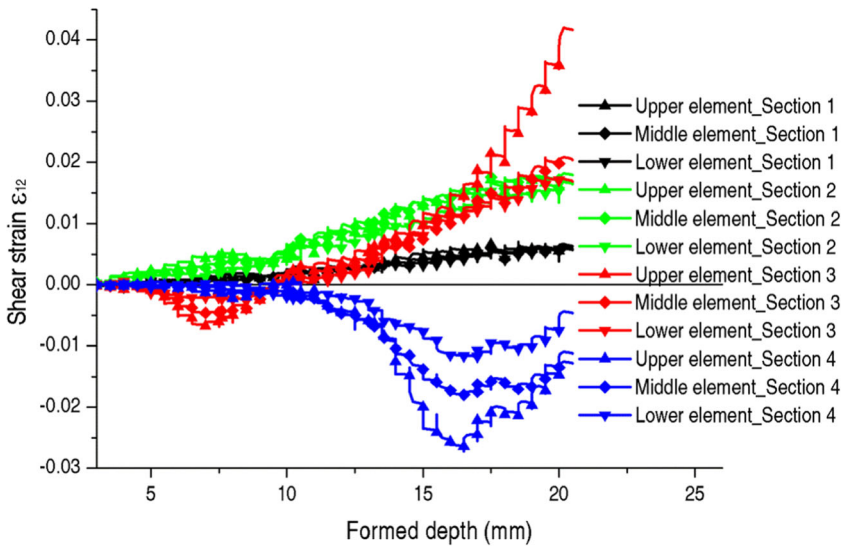

Fig. 17 In-plane shear strain evolution during cone-forming process for upper, middle and lower elements from sections 1 to 4

Table 2 FE simulation details

Test no.	Wall angle (deg)	Step-down (mm)	Sheet thickness (mm)	Tool diameter (mm)	Formed depth (mm)	CPU time (h)
1	60	0.5	1.6	30	20	103
2	60	1	1.6	30	40	200
3	60	2	1.6	30	40	139
4	60	4	1.6	30	40	70

sheet formability will be reduced accordingly. Therefore, small step depth values should be avoided in consideration of the formability. As suggested in the present FE simulation, a step-down size of 2 mm is preferred in consideration of the strain level and formability.

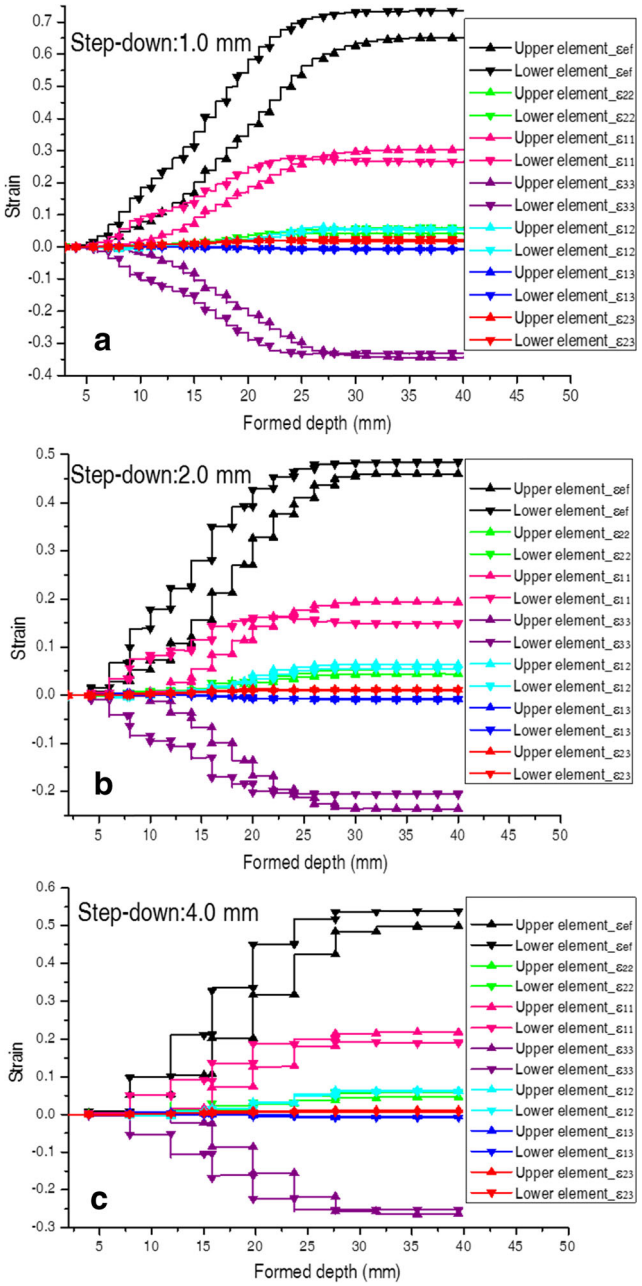

Fig. 18 Strain evolution history with different step-down sizes, **a** 1, **b** 2 and **c** 4 mm

5 Conclusions

In the present work, FE models with fine solid elements for the cone-forming process have been established to investigate the deformation mechanism. Firstly, the FE model is verified by experimental work through the comparison of forming forces. It is confirmed from FE simulation that the deformation behaviour in the ISF process is a combination of stretching, bending and shearing. In addition, the contribution of each strain component to the effective plastic strain during cone-forming process is discussed. Specifically, direct strain perpendicular to the tool motion is the major deformation mode in the cone-forming process. This direct strain could be accumulated to a large value, whilst strain in the forming direction only alternates at smaller values. Strain values at both surfaces depend on the bending direction of the sheet. For the material around the bottom of the cone, larger strain values are obtained at the lower surface, which is consistent with the experimental observation that cracks tend to occur at the lower surface. Shear strain in the forming direction (ε_{23}) prevails greatly amongst the three shear components, and the maximum value occurred in the middle of the sheet. It is also found that the in-plane shear strain is not

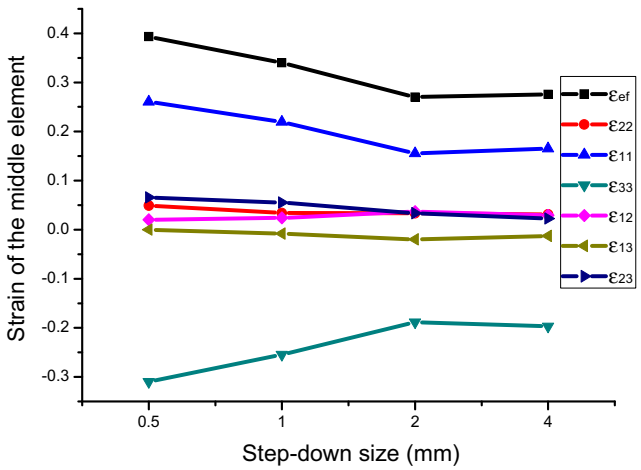

Fig. 19 Comparison of strain values for the middle element at section 3 with four different step-down sizes at the forming depth of 20 mm

negligible, especially at the upper surface. Finally, it is also found that the selection of step-down size could affect the magnitude of effective strain when the same geometric part is deformed.

Acknowledgments The present work was supported by Australian Research Council (ARC) Linkage project. The first author was also supported by 'The Fundamental Research Funds of Shandong University' and 'China Postdoctoral Science Foundation funded project'.

References

1. Jeswiet J, Micari F, Hirt G, Bramley A, Duflou J, Allwood J (2005) Asymmetric single point incremental forming of sheet metal. Annals of CIRP—Manufacturing Technology 54(2):623–649
2. Araghi BT, Göttmann A, Bambach M, Hirt G, Bergweiler G, Diettrich J, Steiners M, Saeed-Akbari A (2011) Review on the development of a hybrid incremental sheet forming system for small batch sizes and individualized production. Prod Eng 5(4): 393–404
3. Silva MB, Nielsen PS, Bay N, Martins PAF (2011) Failure mechanisms in single-point incremental forming of metals. Int J Adv Manuf Technol 56(9):893–903. doi:10.1007/s00170-011-3254-1
4. Silva MB, Skjoedt M, Martins PAF, Bay N (2008) Revisiting the fundamentals of single point incremental forming by means of membrane analysis. Int J Mach Tools Manuf 48(1):73–83. doi:10.1016/j.ijmachtools.2007.07.004
5. Silva MB, Skjoedt M, Atkins AG, Bay N, Martins PAF (2008) Single-point incremental forming and formability-failure diagrams. J Strain Anal Eng Des 43(1):15–35
6. Jackson K, Allwood J (2009) The mechanics of incremental sheet forming. J Mater Process Tech 209(3):1158–1174. doi:10.1016/j.jmatprotec.2008.03.025
7. Kim TJ, Yang DY (2000) Improvement of formability for the incremental sheet metal forming process. Int J Mech Sci 42(7):1271–1286. doi:10.1016/s0020-7403(99)00047-8
8. Jeswiet J, Young D (2005) Forming limit diagrams for single-point incremental forming of aluminium sheet. Proc Inst Mech Eng B J Eng Manuf 219(4):359–364. doi:10.1243/095440505x32210
9. Lu B, Fang Y, Xu DK, Chen J, Ou H, Moser NH, Cao J (2014) Mechanism investigation of friction-related effects in single point incremental forming using a developed oblique roller-ball tool. Int J Mach Tools Manuf 85(0):14–29, **doi:http://dx.doi.org/10.1016/j.ijmachtools.2014.04.007**
10. Xu D, Wu W, Malhotra R, Chen J, Lu B, Cao J (2013) Mechanism investigation for the influence of tool rotation and laser surface texturing (LST) on formability in single point incremental forming. Int J Mach Tools Manuf 73(0):37–46, **doi:http://dx.doi.org/10.1016/j.ijmachtools.2013.06.007**
11. Emmens WC, Boogaard AH (2008) An overview of stabilizing deformation mechanisms in incremental sheet forming. J Materials Processing Tech 209(8):3688–3695. doi:10.1016/j.jmatprotec.2008.10.003
12. Mirnia MJ, Dariani BM (2012) Analysis of incremental sheet metal forming using the upper-bound approach. Proceedings of the Institution of Mechanical Engineers. Part B, Journal of Engineering Manufacture
13. Li Y, Liu Z, Lu H, Daniel WJT, Liu S, Meehan P (2014) Efficient force prediction for incremental sheet forming and experimental validation. The International Journal of Advanced Manufacturing Technology:1–17. doi:10.1007/s00170-014-5665-2
14. Li Y, Daniel WJT, Liu Z, Lu H, Meehan PA (2015) Deformation mechanics and efficient force prediction in single point incremental forming. Journal of Materials Processing Technology (0). doi:http://dx.doi.org/10.1016/j.jmatprotec.2015.02.009
15. Eyckens P, Belkassem B, Henrard C, Gu J, Sol H, Habraken AM, Duflou JR, Van Bael A, Van Houtte P (2011) Strain evolution in the single point incremental forming process: digital image correlation measurement and finite element prediction. Int J Mater Form 4(1): 55–71
16. Lasunon O, Knight WA (2007) Comparative investigation of single-point and double-point incremental sheet metal forming processes. Proc Inst Mech Eng B J Eng Manuf 221(12):1725–1732. doi:10.1243/09544054jem865
17. Yamashita M, Gotoh M, Atsumi S-Y (2008) Numerical simulation of incremental forming of sheet metal. J Mater Process Technol 199(1–3):163–172. doi:10.1016/j.jmatprotec.2007.07.037
18. Ma LW, Mo JH (2008) Three-dimensional finite element method simulation of sheet metal single-point incremental forming and the deformation pattern analysis. Proceedings of the Institution of Mechanical Engineers Part B-Journal of Engineering Manufacture 222(3):373–380. doi:10.1243/09544054jem957
19. Dejardin S, Thibaud S, Gelin JC, Michel G (2010) Experimental investigations and numerical analysis for improving knowledge of incremental sheet forming process for sheet metal parts. J Mater Process Technol 210(2):363–369. doi:10.1016/j.jmatprotec.2009.09.025
20. Smith J, Malhotra R, Liu WK, Cao J (2013) Deformation mechanics in single-point and accumulative double-sided incremental forming. The International Journal of Advanced Manufacturing Technology:1–17. doi:10.1007/s00170-013-5053-3
21. Liu Z, Li Y, Meehan P (2013) Experimental investigation of mechanical properties, formability and force measurement for AA7075-O aluminum alloy sheets formed by incremental forming. Int J Precis Eng Manuf 14(11):1891–1899. doi:10.1007/s12541-013-0255-z
22. Li Y, Liu Z, Daniel WJT, Meehan PA (2014) Simulation and experimental observations of effect of different contact interfaces on the incremental sheet forming process. Mater Manuf Processes 29(2): 121–128. doi:10.1080/10426914.2013.822977
23. Durante M, Formisano A, Langella A, Capece Minutolo FM (2009) The influence of tool rotation on an incremental forming process. J Mater Process Tech 209(9):4621–4626
24. Hamilton KAS (2010) Friction and external surface roughness in single point incremental forming: a study of surface friction, contact area and the 'orange peel' effect
25. Duncan JL, Hu SJ, Marciniak Z (2002) Mechanics of sheet metal forming, vol Book, Whole. Butterworth-Heinemann, Oxford
26. Montanari L, Cristino VA, Silva MB, Martins PAF (2013) A new approach for deformation history of material elements in hole-flanging produced by single point incremental forming. Int J Adv Manuf Technol 69(5–8):1175–1183. doi:10.1007/s00170-013-5117-4